Advanced Shadow Detection and Removal in RGB images: A Novel Approach using Adaptive Wavelet Thresholds and Neural Networks

Dr. Ajay Kumar Boyat

Freelance Researcher,
Ex. Assistant Professor (Senior Grade),
Department of Electronics Engineering, Medi-Caps University, Indore, India.
Ex. Research Scholar,
Research Center, Military College of Telecommunication Engineering, Military Headquarters of Warfare (Mhow), Devi Ahilya Vishwavidyalaya (D.A.V.V.), Indore, India.

ABSTRACT-

Shadow detection and removal are critical tasks in various image processing applications, for example object recognition, tracking, and segmentation. This work presents a novel approach for advanced shadow detection and removal from RGB images using adaptive wavelet thresholds and neural networks. The proposed method converts a color image inform of the HSV color space and employs small image patches for shadow detection. Adaptive wavelet thresholds were used to identify shadow regions, and a neural network with nonlinear regression of the hidden layers and linear regression in the output layer were utilized for shadow removal. This method also incorporates noise reduction using median filtering in the spatial and temporal domains. The experimental results demonstrate the effectiveness of the proposed approach for shadows detecting and removing shadows under various conditions. A comparative analysis of state-of-the-art algorithms, including chromacity-based, Huang and Chen's algorithm, Hsieh et al.'s method, and texture-based methods, highlights the quality performance of the proposed technique. The method achieves high accuracy in shadow detection and removal while preserving the image quality. Furthermore, the proposed approach is computationally efficient and robust to different types of shadows, such as soft and hard shadows, under various illumination conditions. The integration of adaptive wavelet thresholds and neural networks provides a powerful framework for advanced shadow detection and removal from RGB images, making it suitable for a many applications in computer vision and image processing.

Introduction-

Shadow removal is performed by adding and multiplying some constants in the shadow region [1]. Advanced shadow detection and shadow removal from RGB images is a challenging task of computer vision and image processing. The proposed novel approach combines adaptive wavelet thresholds and neural networks to effectively identify and eliminate shadows while preserving the image details. This method first converts the RGB image into the HSV color space and employs small image patches for shadow detection. Adaptive wavelet thresholds were then applied to identify potential shadow regions. A neural network architecture with nonlinear regression in the hidden layers and linear regression in the output layer was used for shadow removal. The network was trained on shadow and non-shadow image patches to determine the optimal shadow removal parameters. Additionally, median filtering is incorporated in both the spatial and temporal domains to reduce noise. The experimental performance output

demonstrates the effectiveness of this approach in accurately detecting and removing both soft and hard shadows under varying illumination conditions, outperforming well known state-of-the-art methods. The integration of adaptive wavelet analysis and neural networks provides a robust and computationally efficient framework for advanced shadow processing of RGB images.

Object recognition is of great interest in many image analysis and processing applications. Recent literature has accepted the general method of deshadow of color images, as follows:

1. The Shadowed RGB color component images with salt-and-pepper noise were processed using a wavelet-based median filter.
2. The average color component is computed using binary and morphological functions. A hypothesis test was applied to detect the shadows.
3. Finally, an energy function was applied to remove shadows from the image [2].

These methods help to understand the scene content. Content-based retrieval from databases is a useful method for shadow detection and removal. Primary color-based imaging, in addition to texture features, is a prominent cue in shadow detection. The characteristics of the color bands were the main gradients when collecting the information.

The patterns of shadows depend on the size of the objects and the angle of the lighting source. This causes problems with scene understanding, object extraction, and tracking. However, the effect of shadows obscures useful information in the image. Several suggested methods have demonstrated the presence of shadows in a visual scene. These methods help minimize the effects of shadows in the image frame sequence. These techniques aim to improve the performance of shadow detection and removal combinedly for computer vision algorithms and enhance the quality and accuracy of object detection and tracking in various applications.

Keywords: Shadow detection, RGB images, Adaptive wavelet thresholds, Neural Networks, HSV color space, and Median filtering

Literature Survey- Tiwari et al. distinguished the survey paper of shadow detection and shadow removal in image and video sequences using various current methods. They also took the indoor and outdoor scenes, fixed and moving camera, umbera, and penumbra shadows in their analysis [3]. Multiple objects can be connected through shadows and create confusion when distinguishing objects in an object recognition system. They differ in foreground and background images based on illumination assessment [4]. Shadow detection and removal are important tasks that have been used for computer vision such as video supervision and scene description [5]. They preserve shadow attributes using a convolutional neural network [6]. No prior was required to measure the image data sequences. Every image sequence has specific properties, such as chromacity and intensity [7]. Paul Dare [8] has explored chromacity based method for shadow images. He applied thresholding at a predefined level and segmentation during postprocessing operations. Tsai [9] has explored colour spaces of hue-saturation-value (HSV), hue-Chromacity based method-value (HCV), hue-saturation-intensity (HSI), luma-in phase-quadrature components (YIQ) and luma-blue of red chromacity based method components. They used YCbCr models with shadow properties in the chromacity-based methods. HSV color spaces were drawn by Krishna et al. [10] and Otsu thresholding was used for shadow removal.

Ref. [11] developed the idea that shadows has removed by minimizing the entropy. A one-dimensional projection is used to distribute the pixel information. The point of consideration is that they referred to an invariant image with minimal entropy dissipation. [12] retains the monochromacity-based method and is more time-consuming than color information. Using the concepts of [12] and Zhu et al. [13], they jointly proposed that shadow-variant near-black features are added to graph cut steps. Prati et al. [14] deploy robust tracking systems and illustrated that the following case studies

(I) The picture shows that few people are closely joined together and cast shadows appear.

(II) Based on the appearance model of each person, various shadow pixels are mixed to obtain the final shadow attribute. This model decreases the reliability of the recovered features inside the shadow region.

Ref. [15] has taken care of all those things that have happened in the review of [14] and concluded that removing shadow mechanisms has a significant impact on the intermediate step (an unavoidable step of threshold selection).

From this perspective, we describe this study in the following sections. In Section 1, the main features of the proposed shadow detection and removal methods are presented. In Section 2, we discuss the implementation and the results.

We compare the state-of-the-art methods with the proposed method in Section 3. Finally, we present conclusion in Section 4.

SECTION 1.

Proposed Method: When light falls upon objects of interest, the intermediate obstruction creates shadows while capturing the scene. An object can then cast a shadow. Intensity-based hard and soft shadows were observed during the image processing. Soft shadows retain useful information about the texture available in the background portion, whereas hard shadows create a dark scene and give little texture. Therefore, the detection of shadows in hard region is a complex process, as it has dark objects in the scene.

This work presents a comparative performance evaluation of innovative techniques for color-based shadow detection. Hence, identified shadow detection and shadow removal as a critical step in the improvement of object detection and tracking. Prominent methods across the world are categorized and compared quantitative performance measures, such as discrimination rates and color desaturation, with qualitative observations.

The proposal addresses the strict assumptions considered in Hsieh et al. [42]. However, the earliest approach is not generalizable for various environments. They proposed a straightforward work when considering the object of interest. The chromacity-based method is the fastest while computing, but it is hard to remove noise and mildly effective in low-resolution scenes. The Huang and Chen method [23] improves the computing accuracy by adapting local region patch shadow models but fails while dealing with the spectral components of the objects that are the same as those available on the background.

The small-region of texture-based technique is robust because it considers neighborhood pixels. However, it may require a longer implementation time. However, this is computationally expensive. Large-region texture-based techniques have yielded accurate results. Owing to the multiple processing steps involved, a significant computational discrepancy was observed in [16].

Here, we compare four methods: the chromacity-based method, Hsieh et al. [42], Huang and Chen's method [23], and texture [16] with some classified methods having features such as spatial and temporal coefficients [14]. We extended this work using wavelet regression analysis in a neural network, and some noise was reduced by the median filter in the spatial and temporal domains. These features have shown a greater impact in the wavelet domain and are helpful for detecting and removing shadows. We split the frequencies into illumination and intensity parts separately. In most cases, the appearing shadow of an object is detected using foreground attributes. However, no shadow was considered in the background. Subtraction and image segmentation were employed during this operation. The shadows are interrupted from the brightness part; therefore, in our proposal, we used uniform and ambient illumination to limit the dark part. This procedure predicts regions under shadows and reduces the intensity in non-shadowed areas.

In this study, shadow patterns were profound by wavelet temporal filter coefficients. These coefficients were obtained using an adaptive wavelet transform. Temporal coefficients provide enhanced results compared with intensity features [16]. Color spaces with separate intensity features were examined using HSV principles [17], [18], and normalized RGB [19]. The proposed method is robust to shadow detection. We adopted the intensity-based HSV method that fully depends on small shadow patches (image patches in clusters developed using the non-local mean algorithm). We also interpret that brightness, background, foreground, and shadow do not individually manipulate the HSV components under the satisfaction of the three conditions.

$\beta_1 \leq (F^V_{Patch}/B^V_{Patch}) \leq \beta_2$

Therefore, $Patch$ is small patch that contain group of pixels in a cluster, $F$is image, $B$and is background scene of reference image.

$$(F^S_{Patch} - B^S_{Patch}) \leq T_S$$
$$(F^S_{Patch} - B^S_{Patch}) \leq T_H$$

HSV are the hue, value of intensity and saturation of the patch.β_1 and$\beta_2$are adaptive wavelet thresholds which are empirically optimized. $T_S$and$T_H$are chosen thresholds. Different color spaces may not always yield good results in color images [20]. However, a group of pixels in clusters is estimated using a nonlocal mean called a small patch. This can yield more fruitful results and help count the noise.

The Proposed RGB based small patches illustrate the spatial and spectral components of an adaptive wavelet. Otsu thresholding was utilized to reduce the variance in the inter- and intra-class domains. Our proposal splits the cast and self-shadows. Equation shows predefined thresholding levels

$$I_{patch}(i,j) = \begin{cases} 1 & if(i,j) \geq T \\ 0 & if(i,j) \leq T \end{cases}$$

$I_{patch}(i,j)$ is operating shadow patch, i =1…N: number of rows and j =1….M: number of columns in single patch.$T$is chosen threshold. The textures of the small patches are correlated. These are shown in the foreground and background scenes. Small patches are estimated by$patch = (x,y)$ using gradient $\Delta_{patch} = \sqrt{a{\Delta_x}^2 + b{\Delta_y}^2}$ where, $a$and$b$are illumination constant of two consecutive patches. $\Delta_x$and$\Delta_y$two gradient one for horizontal and second for vertical directions of a patch, respectively. The overall magnitude of pixels in each wavelet sub-band is higher than the value of threshold T [15]. Then, pixels are grouped into patches using a nonlocal mean algorithm. The selected patches were examined in a specific direction in the image. However, each patch was selected because of its specific magnitude and angle. Hence, the gradient difference between the foreground and background patches is determined as follows:

$$\Delta\theta_{patch} = arccos \frac{{\nabla_x}^F {\nabla_x}^B + {\nabla_y}^F {\nabla_y}^B}{\sqrt{({\nabla^F_x}^2 + {\nabla^F_y}^2)}\sqrt{a^2+b^2}\sqrt{({\nabla^B_x}^2 + {\nabla^B_y}^2)}}$$

Whereas ${\nabla_x}^F$and ${\nabla_x}^B$ gradient of foreground and background patch in horizontal direction, respectively. ${\nabla_y}^F$and ${\nabla_y}^B$ gradient of foreground and background patch in vertical direction, Correlation among foreground and background patch for a single region as given by:

$$Corr = \frac{\sum_{patch=1}^{n} H(T - \Delta\theta_{patch})}{N}$$

Whereas, $H(.)$is the log normal function instead of unit step function, which is one, if gradient difference among patches is less than or equal to threshold(T), otherwise zero. N is number of pixels in one cluster from selected patches, if$Corr$is higher than T the patch is adopted in shadow area hence, removed.

The mask function$m_{(k1,k2)}$is generated by parallel logical shifting of binary version of gray image for scaling the wavelet coefficients. Patch is illustrated as$patch = (x,y)$. Proposed method was utilized the convolution of $m_{(k1,k2)}$and$patch = (x,y)$. This convolution is smoothen the signal and preserves brightness. This convolution is so called smooth mask and it can represented as $C_{(n1,n2)}$.

$$C_{(n1,n2)} = \sum_{k1=-\infty}^{\infty} \sum_{k2=-\infty}^{\infty} m_{(k1,k2)} * p_{(n1-k1,n2-k2)}$$

Hence, Shadow region in a single patch is obtain using the difference of reference background and average shadow region. The difference was calculated by$D_{patch}(j,k)$.

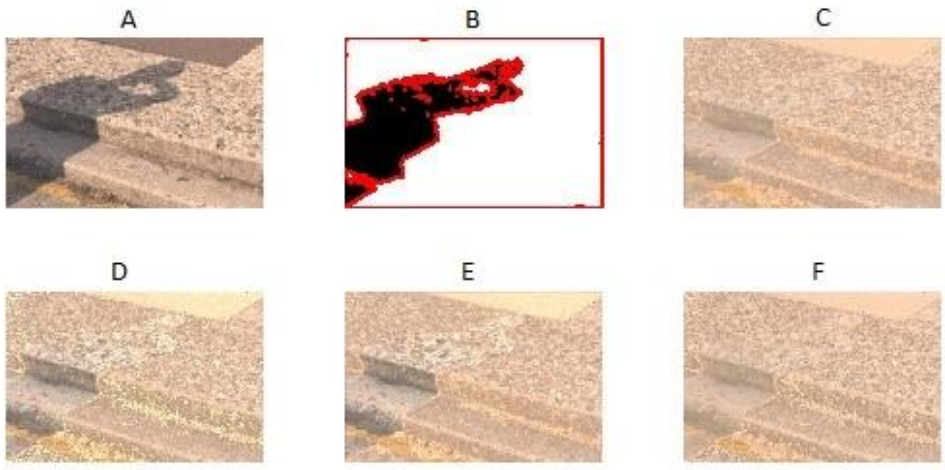

Figure 1 A: Original image, B: Red color edges are shown using boundary segmentation and Diffusion algorithm, C: Added smooth mask$C_{(n1,n2)} * D_{patch}(j,k)$ in RGB channels, D: Multiplying shadow pixels with correction factor$C_{(n1,n2)} * \frac{R_{patch}(j,k)}{S_{avg}}$, E: Higher luminance obtained using subtraction of smooth patches of mask $m_{(k1,k2)}$and F: Additive correction using$m_{(k1,k2)} * D_{patch}(j,k) * \frac{R_{patch}(j,k)}{S_{avg}}$in 'ycbcr' channels.

To obtain the deshadow image, we used $C_{(n1,n2)} * D_{patch}(j,k)$ in the cluster and after this the restored image is more purifying using correction factor$C_{(n1,n2)} * \frac{R_{patch}(j,k)}{S_{avg}}$, this can be seen in Figure 1 and Figure 2.

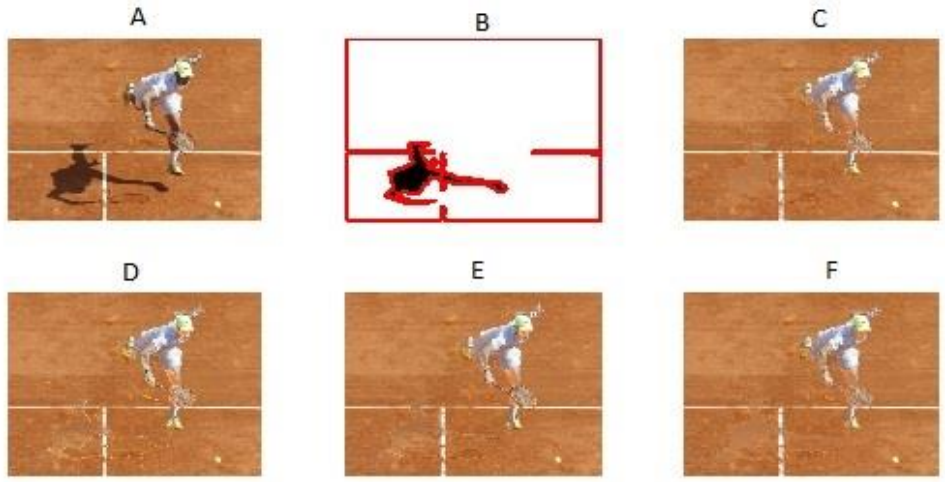

Figure 2 A: Original image, B: Red color edges are shown using boundary segmentation and Diffusion algorithm, C: Added smooth mask$C_{(n1,n2)} * D_{patch}(j,k)$ in RGB channels, D: Multiplying shadow pixels with correction factor$C_{(n1,n2)} * \frac{R_{patch}(j,k)}{S_{avg}}$, E: Higher luminance obtained using subtraction of smooth patches of mask $m_{(k1,k2)}$and F: Additive correction using$m_{(k1,k2)} * D_{patch}(j,k) * \frac{R_{patch}(j,k)}{S_{avg}}$in 'ycbcr' channels.

The ratio of reference background patch and average shadow region is multiplying by $C_{(n1,n2)}$for minimizing the shadow effect. Reference background patch is represented as $R_{patch}(j,k)$. For more accuracy, the RGB image is passed into 'ycbcr' channel. $D_{patch}(j,k)$ is further estimated in 'ycbcr' channel as follows.

$$D_y = R_{patch}(j,k) - S_y$$

$$D_{cb} = R_{patch}(j,k) - S_{cb}$$

$$D_{cr} = R_{patch}(j,k) - S_{cr}$$

Separate difference matrices are found usingD_y, D_{cb} and D_{cr} in 'ycbcr' channel. Further, minimizing the effect of shadow we used the following equation in'ycbcr' channel.

$$m_y * \frac{R_{patch}(j,k)}{S_y}$$

$$m_{cb} * \frac{R_{patch}(j,k)}{S_{cb}}$$

$$m_{cr} * \frac{R_{patch}(j,k)}{S_{cr}}$$

m_y, m_{cb} and $m_{cr}$are the mask in 'y' channel , 'cb' channel and 'cr' channel, respectively. s_y, s_{cb} and $s_{cr}$are the shadow in 'y' channel , 'cb' channel and 'cr' channel, respectively.

This study provides a simple technique for shadow detecting and shadow removing from a single RGB color-based image. The brightness of the image might be nonuniform in a shadow region. A diffusion algorithm was applied along with the shadow boundary. Thus, the proposed method can filter the shadow and reduce the errors that appear in the shadow region. The above tasks are illustrated in Figures 2 and 3.

SECTION 2.

Implementation, Result, and discussion- Chormacity, Huang and Chen's method [23], and texture methods are very costly in terms of mathematical computing time because they use only a single pixel instead of a patch. However, all of these methods are sensitive to noise. Therefore, we employed an adaptive wavelet transform to reduce noise. Our method was more effective under brown background conditions. Moreover, the proposed method is independent of the type of shadow, such as soft and hard shadows, in different projected lights.

Table 1 shows the comparison of chromacity based method, Huang and Chen method [23], Hsieh et al. [42], which is a texture-based method with the proposed method. In Table 1, we list four parameters: color spaces, spatial and temporal verification, and correlation.

Table 1 shows the comparison of Chromacity based method, Huang and chen method [23], Hsieh et al. [42], texture based methods with proposed method.

Observations	Chormacity method	Huang and chen [23] method	Hsieh et al. [42] method	Texture based method	Proposed method
Color spaces	HSY, Normalized RGB and YUV [17,19,22,]	DiChromacity based method and general RGB [23,24,25]	Head detection based on RGB [23]	2D RGB model [37]	HSY, Normalized RGB and YUV
Spatial and temporal verification	Not applicable [24,40]	Using Gaussian mixture model [24,40]	Spatio-tempo test done using intensity and location [38,23,39]	Spatio-tempo test done using colour segmentation [24,25,34,35]	Spatio-tempo test done using applied on small patches [38,23,39]
Correlation	Works on pixels [20,41]	Pixel and small regions Using Gradient and Markov random fields [24,36]	Pixel and small regions Using Oriented gradient and vanishing points[21,33]	Pixel and small regions Using gradient and PCA methods [20,41]	Pixel and small regions Using gradient and adaptive wavelet based median transform
Computation time	18msec.	20.02msec.	24.5msec.	24.3msec.	21.07msec.

HSY, Normalized RGB and YUV [17-22] methods are used in the chromacity-based method. The dichromacity-based method and general RGB [23-25] methods are described in Huang and Chen's method [23]. Hence, the Huang and Chen method [23] was slightly better than the chromacity-based method. Hsieh et al. method [42] is taken head detection using RGB model. Therefore, the texture-based method and the proposed method are also used in RGB color models. The proposed method performs a spatiotemporal test using a wavelet-based Gaussian mixture model. In this study, a Gaussian mixture model was applied to small image patches. The intensity of the pixels was taken from [42]. The texture method uses color segmentation. Pixel correlation was performed in the proposed method using the gradient descent method. In this study, we used small color patch-based segmentations for shadow removal.

Chromacity-based methods show the correlation of pixels based on [26-27] utilize Gradient and Markov random fields. Huang and Chen method [23], Hsieh et al. method [42] and texture based method used pixels and small regions. These methods deal with oriented gradients, vanishing points, and Principal Components Analysis (PCA), respectively. In our analysis, the chromacity-based method had the lowest computational time because of the use of pixel-based illumination. Huang and Chen method [23] and proposed method has almost same computing time because taking gradient of small patch of a color shadow image. Hsieh et al. [42] and texture based methods are little complex therefore have more computational time.

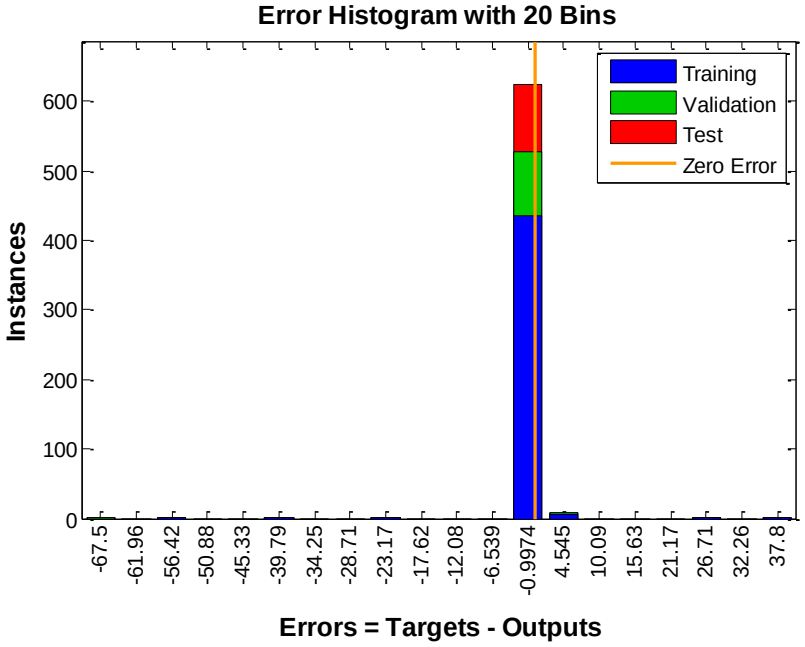

Figure 3 Error histogram show the Neural Network performance during training, validation and testing of 1x64 samples of Output and Target

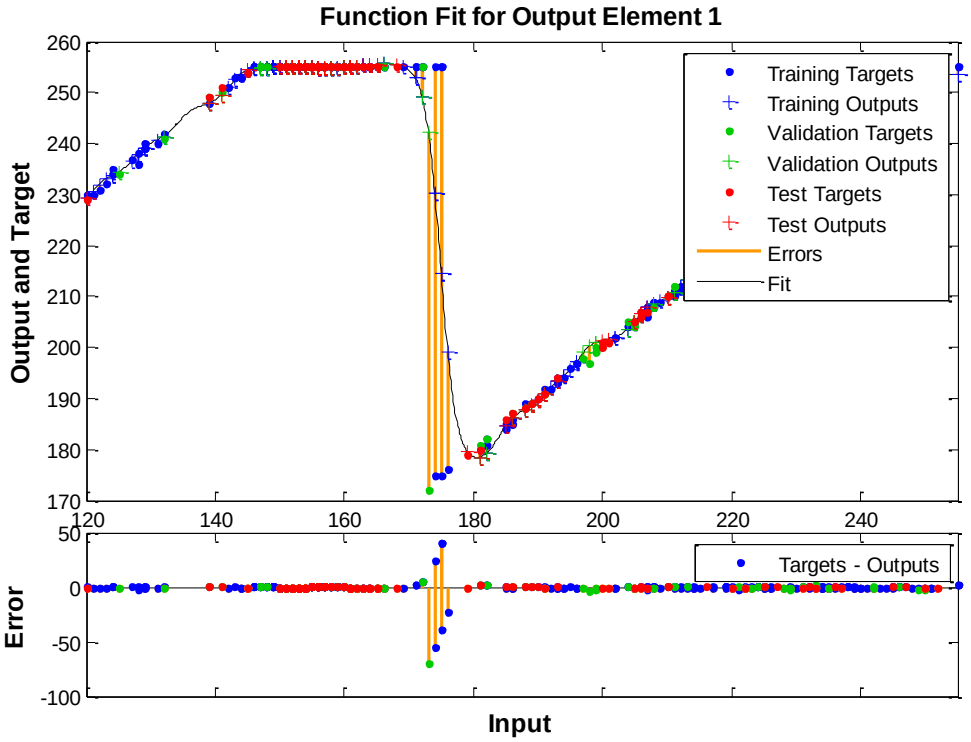

Figure 4 Wavelet Non-linear quadratic regression model of Neural Network deploys in Inputs, Outputs and Targets with Error

The neural Network performance during the training, validation, and testing of 1 × 640 samples of Output and Target are shown in Figure 5 and 6, respectively. We utilized wavelet nonlinear regression in the hidden layer and wavelet linear regression in the output layer of the Neural Network. Twenty hidden layers of wavelet details were used to create the Neural Network. Image patches are fixed on significant values of error falls on -6.39 to +4.54 is shown in Figure 3.

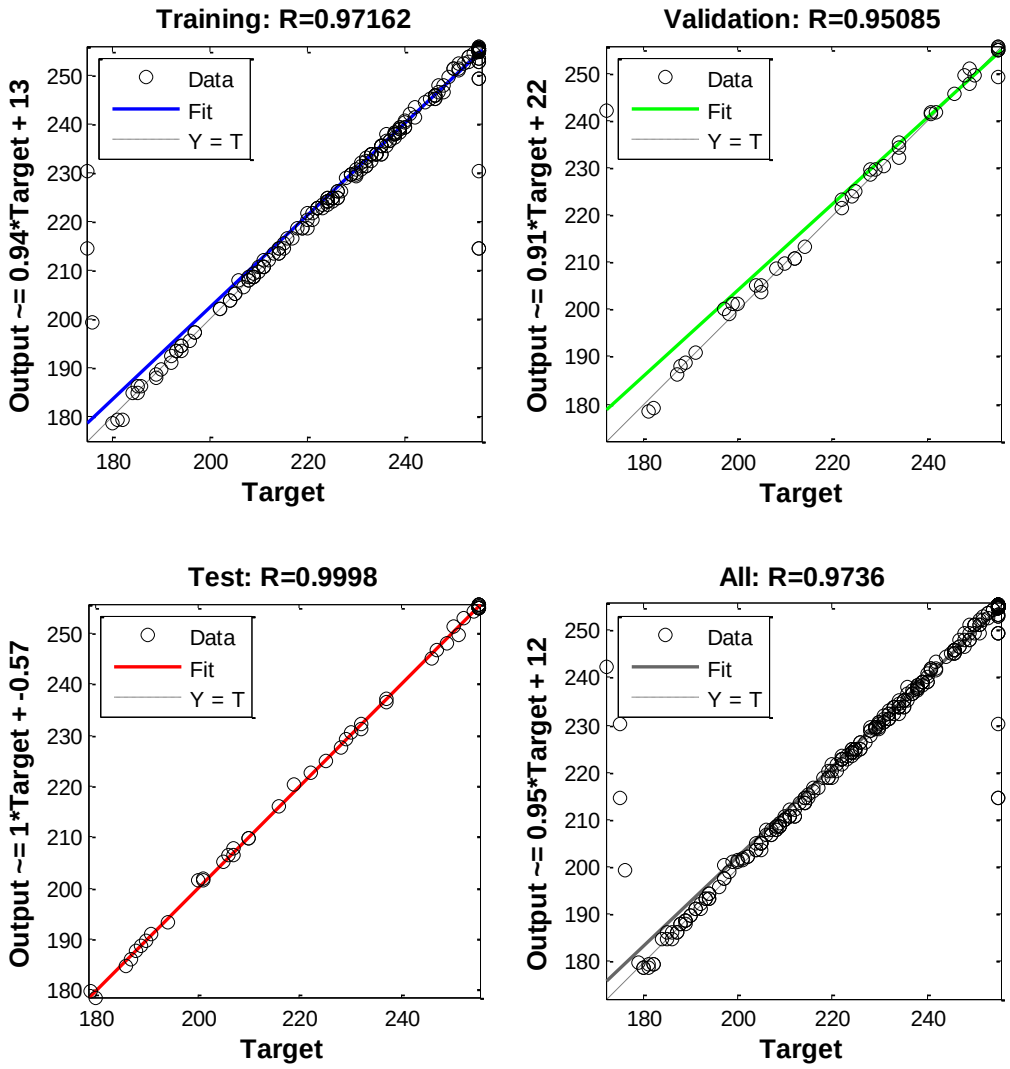

Figure 5 Regression polts display Outputs, R value and Targets

A total of 1 × 640 samples of small patches were collected using the nonlocal clustering method of the original image. In a patch, each sample has a maximum value of 256 because of the grayscale. These samples are used in the curve-fitting function of the wavelet nonlinear quadratic regression model of the Neural Network. The proposed model is deployed in terms of inputs, outputs, and targets with errors, as shown in Figure 4. In our paradigm, if the error is zero, training is initiated. After the last validation period, the testing was started. Figure 4 shows that the training, validation, and testing data were nearly fixed. After 180 input vectors, a perfect convergence of the curve occurred, as shown in Figure 4. The nonlinear regression curve diverges beyond 180 inputs, and it can be said that the validation is stopped here and the neural network needs to be trained again. Figure 4 shows that training, validation, and testing achieved almost the same values. Hence, the nonlinear regression curve was perfectly fitted and fine. Figure 4 shows that the error was almost zero during the training and testing. Regression plots are shown in Figure 5. Despite the Outputs, R values, and targets, the regression curve achieved the best fit.

It has been seen that regression curve is subdivided into four subplots with respect to different inputs. Regression plots started the testing of wavelet-based neural networks that reflect nonlinear regression. Image data patches sustain the wavelet coefficients used in our training and testing analyses. When the target data patches were

different, the input and output images were considered. Therefore, a wavelet-based neural network must be retrained.

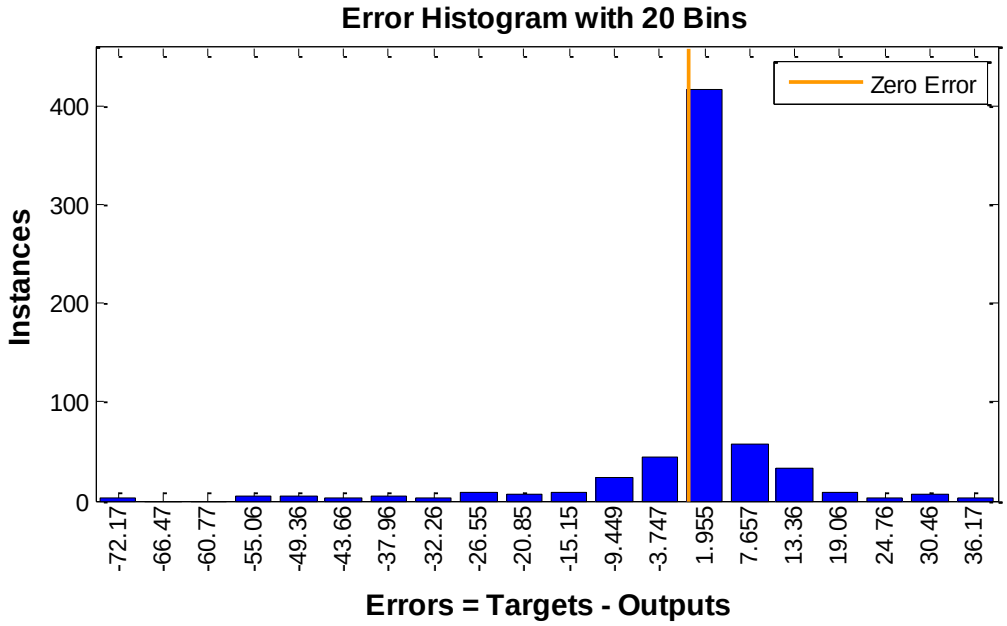

Figure 6 Error histogram show the Neural Network performance during training of 1x640 samples of Output and Target

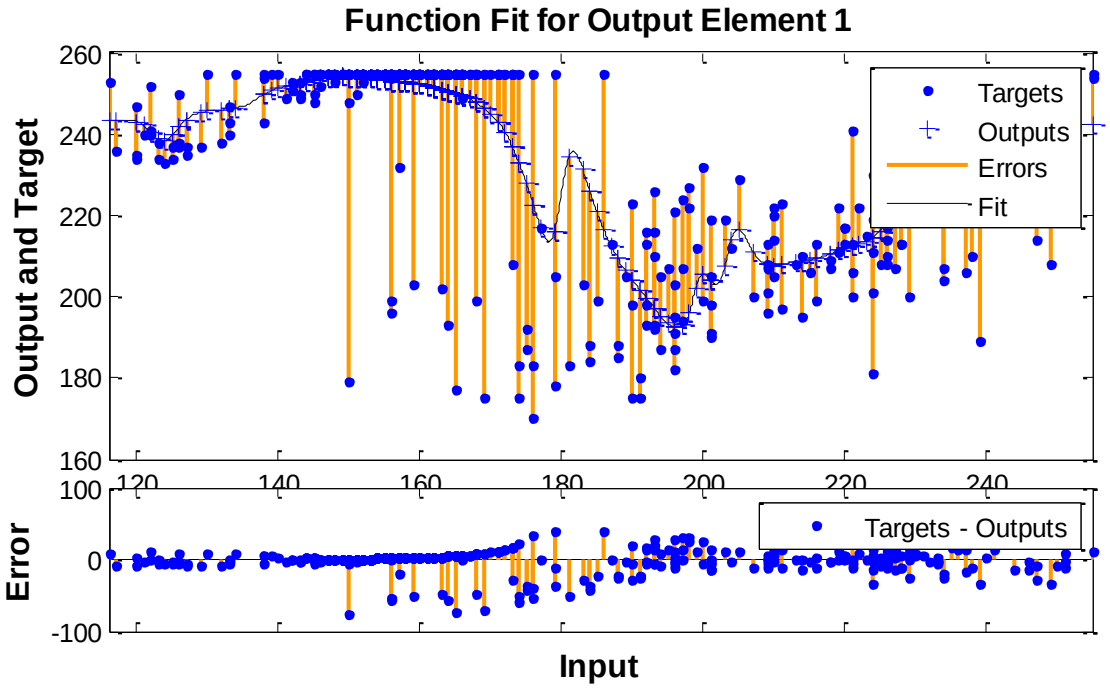

Figure 7 Restored image patch is used in curve fitting function deploys Inputs, Outputs and Targets with Error

Wavelet detail coefficients were obtained using subband coding. Figure 5 also reflects all internal wavelet detail coefficients in linear regression; if the output approaches the target, the average R value is 0.97 of the total response.

In Figure 4, it can be seen that training, validation, and testing were started after taking 200 near the input data values. As shown in Figures 3 and 6, the error histogram is maximum at -0.997 error value. Figure 3 and 6 show perfect histograms for the input and restored images.

Figure 4 and 7 illustrate that the wavelet-based nonlinear regression neural network achieved the same result after training and testing. The restored image is used in the curve fitting function delivered by the nonlinear quadratic regression model and commonly deploys inputs, outputs, and targets with errors. This is illustrated in Fig. 7.

Small regions are converted into large regions, and the proposed method is extended using the HSV character. The purpose is to eventually create large patches in the entire shadow. The classified small shadow pixels impose an upper bound on the detection accuracy. Misclassification of object pixels results in false shadow patches. Object pixels were used, as in the shadow regions of concern. To avoid this, we implemented the optional step illustrated in [28], where shadow patches are breaks in the edges and foreground scenes. Figure 5 and 8 show similar results for both the input and the target (restored image). Figure 8 represents gradient, μ (mu) and validation fail curve at 6 iterations during training of wavelet neural network. The data converged as the number of iterations increased. This can be observed in Fig. 8. The wavelet-neural-network-based regression curve achieved 99% accuracy after three iterations. This can be observed in Figure 9. The Mean Square Error (MSE) is shown in Figure 10. At the third epoch, the MSE was very low, after which it was constant. Hence, it can be said that the MSE decreased in all cases.

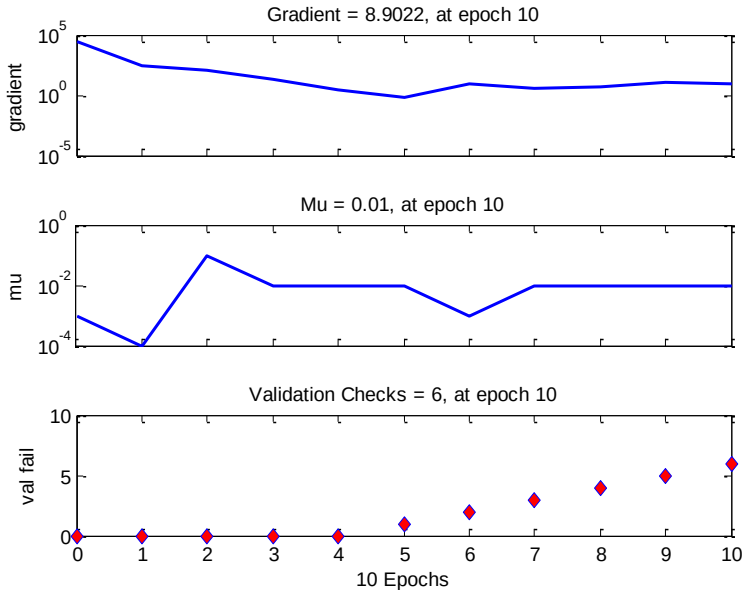

Figure 8 Gradient, mu, and validation fail curves at nine iterations during training of the wavelet neural network.

Every shadow frame sequence was observed to detect shadow performance. Table 2 shows the performance of Training, Validation and Testing of the wavelet neural network-based nonlinear regression in terms of MSE and Fitting accuracy. In Table 2, it can be seen that the accuracy of the fitting curve is approximately 99.97% at tenth patch recording. The training, validation, and test (MSE) data are separately shown at the fourth epoch. This is illustrated in Figure 10. A slight decrease in the fitting accuracy was observed during the validation and testing steps. However, the proposed model automatically selected 96 out of 640 samples in a single patch. The potential literature described in this paper requires more operational steps to estimate central moments and upgrade the shadow model.

Figure 11–14 show that the color features and locally adaptive temporal filtering coefficients perform better. Huang and Chen [23], and chromacity-based methods that use large texture-based regions. They showed a lower hue and saturation. The large-region texture-based method yields superior results. Therefore, similar small patches were converted into larger patches. Figure 11–14 present the binary images obtained from segmentation. However, the Otsu algorithm does not propound the opportunity to retrieve large patch shadows; therefore, we used a small patch shadow. The filtering process was used to reduce the artifacts. Shadows that caused confusion were dismissed.

Noise Removal- This study deals with salt-and-pepper noise-corrupted images, as shown in [26-27]. Therefore, noise estimation is performed using the noise variance of salt-and-pepper noise and successfully evaluated using the methods in [29-32], as illustrated in Fig. 1, 2, 3, 12, and 13.

First wavelet transform subdivided the noisy image $Z_{patch}(j,k)$ in approximation and detail using small patch. All operations were designed on a small patch instead of the entire image, resulting in less time consumption and better restored images. The proposed method utilizes a pattern-recognized neural network with a higher accuracy. In the proposed method, the detailed components are set to zero. Furthermore, the approximation part is analyzed with the median filter. The below equations represent the proposed method:

$Z_{patch}(j,k) = D[f(j,k)] + I_{patch}(j,k)$ Where $f(j,k)$ is original image, $I_{patch}(j,k)$ is Noise image, $Z_{patch}(j,k)$ is degraded image and degrading function is D.

Table 3 Performance of Training, Validation and Testing of wavelet neural network based non-linear regression in terms of MSE and Fitting accuracy

Performance	MSE					Fitting accuracy of Non-linear regression					Samples obtained from
Training	33.45	44.11	45.76	18.64	61.32	95.57	94.56	94.23	97.79	92.28	First matching patch
Validation	126.85	44.19	20.02	115.26	5.10	87.23	94.30	97.33	84.51	99.22	
Testing	15.13	44.59	90.43	123.16	23.04	98.30	94.14	90.05	82.96	97.45	
Training	8.51	13.43	8.16	14.90	16.91	98.95	98.47	99.06	98.20	98.09	Second matching patch
Validation	38.05	1.48	1.97	5.25	6.22	96.91	99.83	99.96	99.94	99.41	
Testing	19.37	3.77	66.15	2.45	6.61	97.87	99.96	94.70	99.77	99.20	
Training	32.63	65.24	17.75	40.01	60.18	96.22	91.61	97.92	95.43	92.38	Third matching patch
Validation	96.95	5.18	188.29	2.55	27.94	85.28	99.48	76.18	99.69	96.98	
Testing	3.28	6.38	1.12	69.68	118.56	99.64	99.41	99.89	89.93	88.89	
Training	91.57	51.75	66.10	33.34	70.11	91.35	94.66	93.12	96.75	92.29	Fourth matching patch
Validation	57.24	123.12	74.35	76.71	21.14	92.35	87.12	89.95	91.11	97.93	
Testing	27.25	1.36	119.02	92.38	36.14	95.96	99.84	89.29	86.48	95.17	
Training	33.44	117.12	42.92	39.85	27.06	96.34	88.67	95.43	95.98	96.98	Fifth matching patch
Validation	12.07	3.69	83.89	20.85	17.67	98.78	99.69	92.89	97.94	98.55	
Testing	180.31	9.88	97.47	142.50	212.29	85.49	99.07	88.93	84.23	78.88	
Training	44.67	54.80	72.45	60.40	60.20	95.92	94.90	93.27	93.76	93.93	Sixth matching patch
Validation	2.93	70.60	7.13	68.60	11.54	99.71	93.20	99.24	93.97	99.18	
Testing	155.60	17.36	17.36	39.67	6.15	84.06	98.18	98.51	97.36	99.31	
Training	82.64	33.05	47.14	48.86	22.74	89.23	95.16	93.38	93.81	96.94	Seventh matching patch
Validation	49.02	23.41	1.61	43.52	40.94	91.20	97.85	99.80	99.94	94.87	
Testing	95.68	10.06	57.54	51.14	14.11	86.28	98.87	92.14	89.96	98.28	
Training	35.46	41.00	31.60	24.61	44.15	93.93	93.04	94.66	96.16	93.62	Eighth matching patch
Validation	16.59	11.77	31.12	6.12	6.32	97.58	98.60	96.13	99.25	98.81	
Testing	42.74	1.77	51.47	94.66	17.22	95.08	99.73	92.46	86.26	97.24	
Training	27.40	38.23	32.87	14.37	42.74	97.25	95.70	96.43	98.33	95.08	Ninth matching patch
Validation	3.26	9.56	5.56	1.20	32.78	99.62	99.07	99.64	99.98	96.35	
Testing	57.71	60.90	31.93	140.30	23.75	91.99	94.53	96.66	89.05	98.46	
Training	20.57	26.43	16.64	24.41	21.13	97.61	96.88	98.08	97.07	97.43	Tenth matching patch
Validation	52.40	16.33	2.79	9.66	32.64	95.08	98.5	99.96	98.94	96.94	
Testing	2.36	6.26	67.91	24.07	42.41	99.97	99.94	90.00	97.91	94.49	

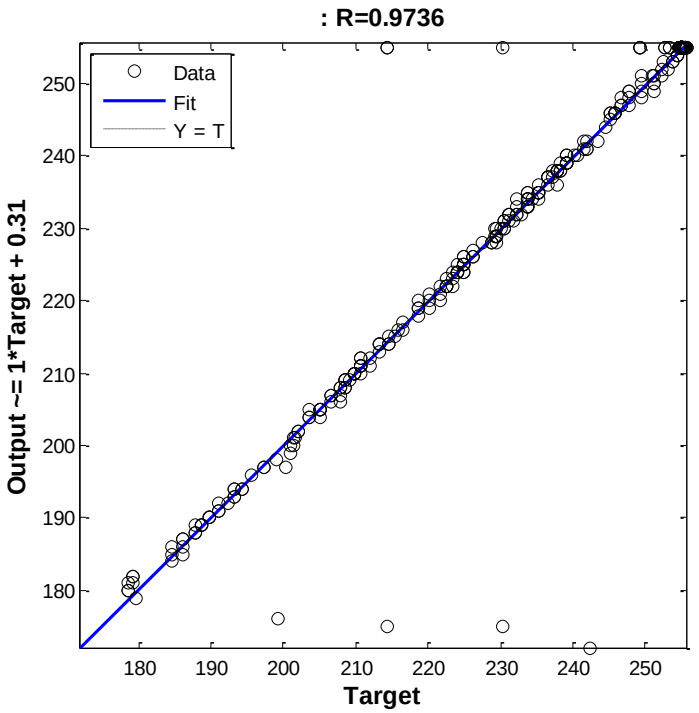

Figure 9 wavelet neural network based non-linear regression curve achieved 99.97% accuracy at 3 iterations during testing

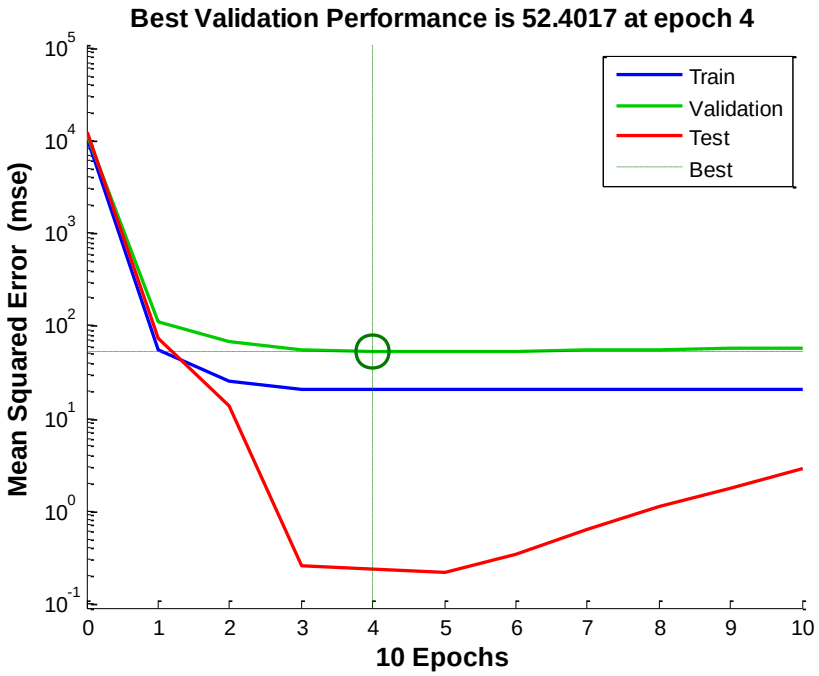

Figure 10 MSE versus performance of wavelet neural network based non-linear regression

$I_{pair}(j,k) \in A \equiv \{1,\ldots\ldots E\}X\{1,\ldots\ldots F\}$ is 1X640 resize gray level small patch. Where $\{1,\ldots\ldots E\}$and $\{1,\ldots\ldots F\}$are the rows and columns, respectively of $I_{patch}(j,k)$. $Z_{patch}(j,k) = \{\ {}^{0}_{1}$

Noisy image $Z_{patch}(j,k)$ identifies intensities of noisy image. For binary images, the following noise intensity values of 0 for black (pepper), and 1 for white (salt).

The (Discrete Wavelet Transform) DWT of degraded image $Z_{patch}(j,k)$ is

$w_{patch}(j,k) = W_{patch}(j,k)Z_{patch}(j,k)$

The approximation and details signals of one patch

$$w_{patch}(j,k) = \{A^d_{2^j}f, D^1_{2^j}f, D^2_{2^j}f, D^3_{2^j}f\}$$

Whereas $A^d_{2^j}f$is the approximation coefficients of low frequencies and $D^1_{2^j}f, D^2_{2^j}f\ and\ D^3_{2^j}f$ are details of the wavelet$w_{patch}(j,k)$ set to zero.

$D^1_{2^j}f$ = 0, $D^2_{2^j}f$ = 0 and $D^3_{2^j}f$ = 0

This image denoising method based on neighbor image patch. Once noisy patches identified it will be removed by median filter in wavelet domain.

Apply median filter upon the approximation wavelet coefficients of small patch using$\hat{v}_{patch} = MED\{A^d_{2^j,1}, A^d_{2^j,2}, A^d_{2^j,3}\ldots\ldots, A^d_{2^j,N}\}, n$ numbers of small patches are summarized and Inverse Discrete Wavelet Transform (IDWT) is taken to get the final restored image.

$$\hat{f}(j,k) = \sum_{patch=1}^{n} W_{patch}{}^{T} w_{patch}(j,k)$$

SECTION 3.

Comparison- In this section, we compare the chormacity based method, Huang and Chen method [23], Hsieh et al. method [42] and texture based method with our proposed method. Our quantitative experiments are summarized all the above four method with our proposal using through qualitative observations. The chromacity based method leads reasonably in few scenes but it is simple and fast [14]. It discriminate the shadow regions with tradeoff between detection and discrimination. The Huang and Chen [23] method is based on learning and adapting using appearances in the background, the so-called moving cast shadows. Hsieh et al. [42] based method uses spectral and texture features with an assumption, the method works independently on object and shadow shape. The chromacity-based method utilizes the brightness of images but is sensitive to pixel-level noise; however, in our method, we could not directly work on pixel intensities, as shown in all state-of-the-art methods.

SECTION 4.

Conclusion-

This paper presents a novel approach for advanced shadow detection and shadow removal from RGB images using adaptive wavelet thresholds and neural networks. A color image is converted in the HSV color components and employs small image patches for shadow detection. Adaptive wavelet thresholds were used to identify shadow regions. In the hidden layers, neural network performs nonlinear regression and linear regression in the output layer were utilized for shadow removal. This method also incorporates noise reduction using median filtering in the spatial and temporal domains. The experimental results demonstrate the effectiveness of the proposed approach in detecting and removing shadows under various conditions. A comparative analysis of state-of-the-art methods, including chromacity-based, Huang and Chen's method, Hsieh et al.'s method, and texture-based methods, highlights the quality performance of the proposed technique in terms of accuracy, computational efficiency, and robustness to different types of shadows under varying illumination conditions. We know that sunlight does not reach the object of interest directly because of the obstructed shadows. The object of interest is also a shadow. We propose an approach for shadow detection and removing in a RGB image. During the operations, the color image is converted to the HSV color space. In this study, we implemented a simple and suitable method according to our objectives. The proposed method was generalized. The results shown in this paper are recognizable for different conditions, and could be improved by adding different assumptions. This indicates that the proposed method is robust under different shadow conditions. We have also worked on texture-based advanced classifier methods. Our method described the spatial and spectral components of shadow images as classified using the chromacity-based and texture methods. We used neural network-based classifiers for the distinguished image. We evaluated a wide range

of training and testing image patches. In this study, each method had its strengths and weaknesses. Most algorithms operate on pixels or regions. Our method works on patches and achieves object tracking, recognition, and segmentation performance. Finally, we conclude that the proposed method is considerably better. It also works with feature-detection algorithms. All of these methods work with the property of preselecting a group of pixels and supplying them to shadow remodeling.

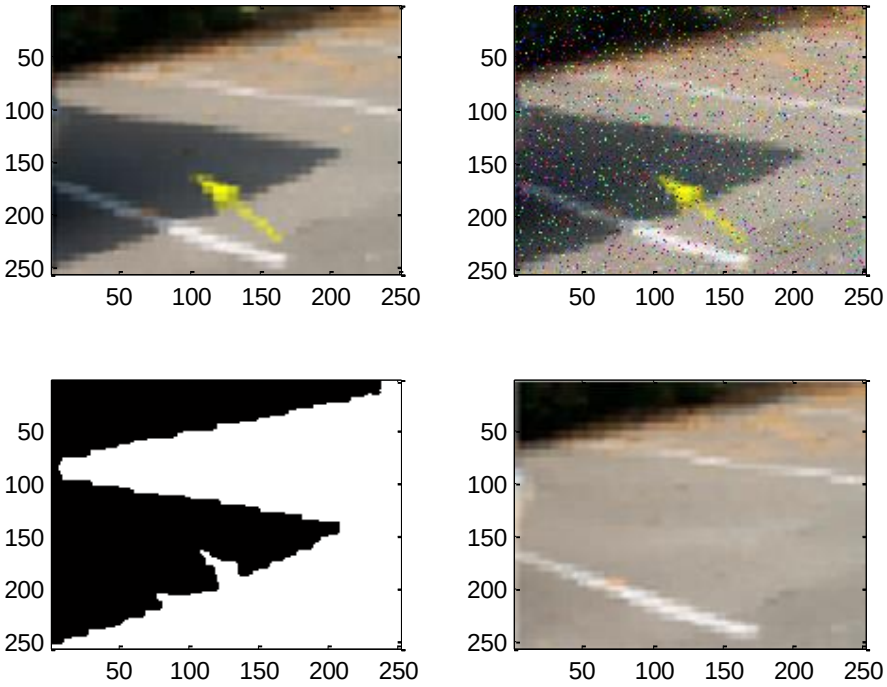

Figure 11 (a) Original color image (b) Image corrupted with salt-and-pepper noise (c) Binary image using segmentation (d) Denoised and deshadow color image by the proposed method.

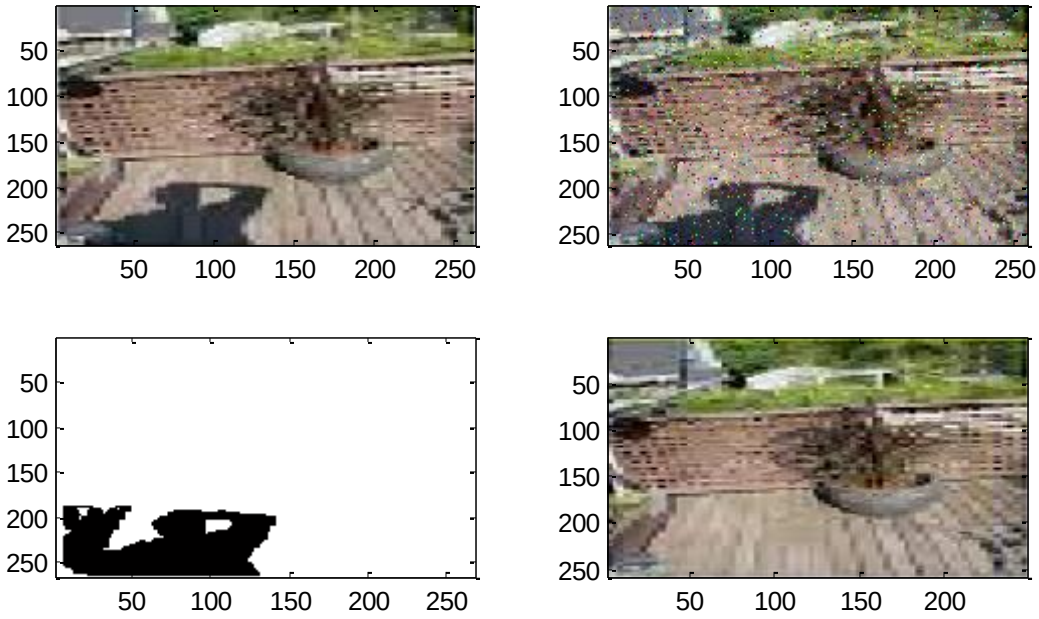

Figure 12 (a) Original color image (b) Image with salt-and-pepper noise (c) Binary image using segmentation (d) Denoised and deshadow color image of the proposed method.

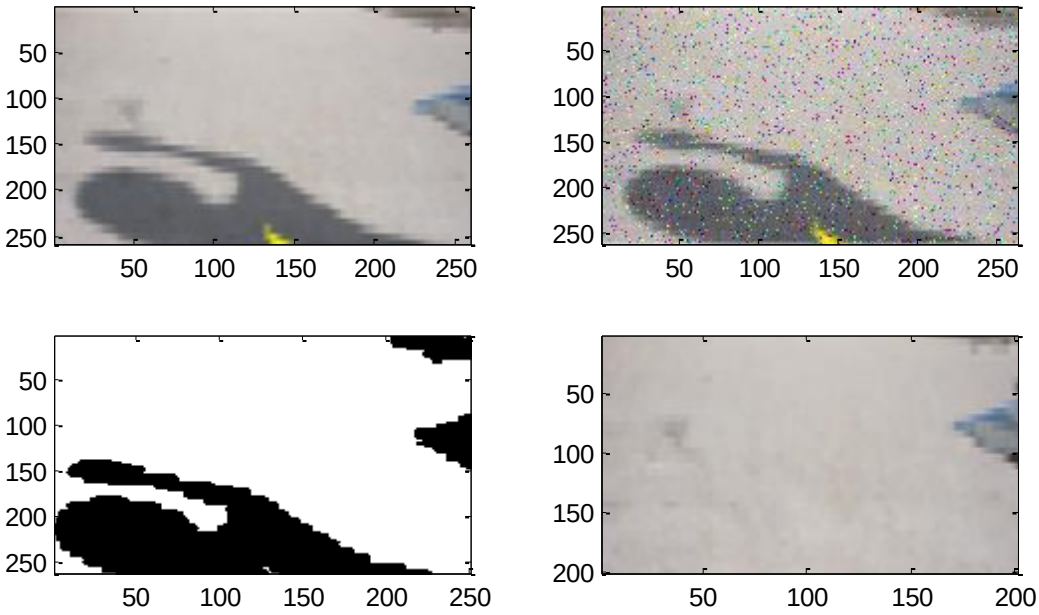

Figure 13 (a) Original color image (b) Image with salt-and-pepper noise (c) Binary image using segmentation (d) Denoised and deshadow color images of the proposed method.

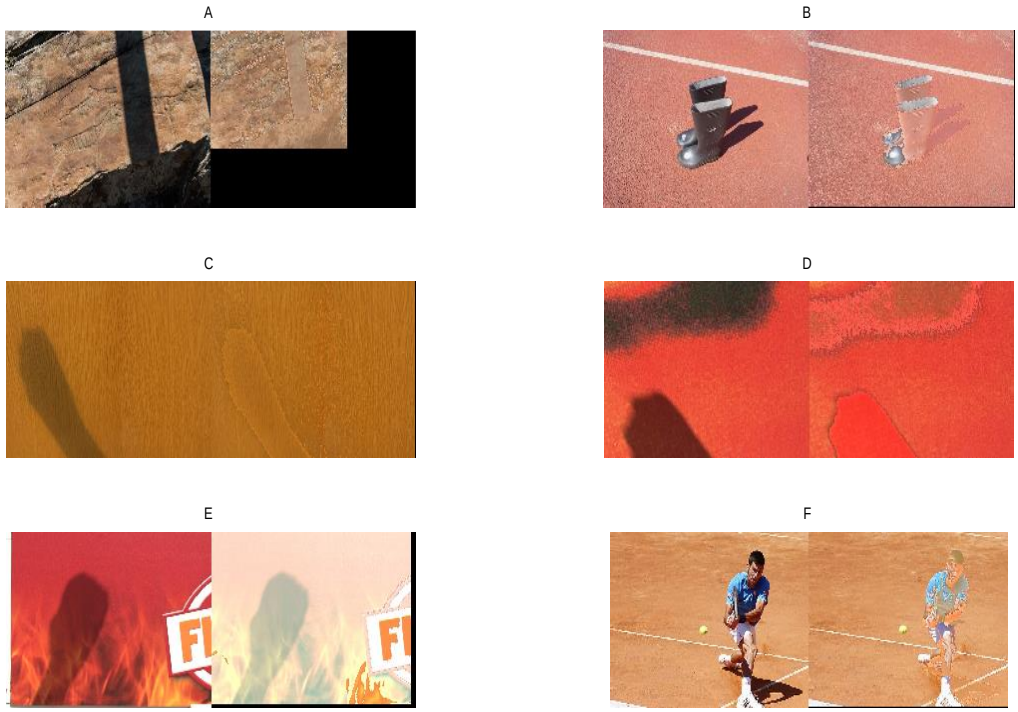

Figure 14 Deshadow by various images using proposed method

References-

[1] Murali, S. and Govindan, V. K. "Shadow Detection and Removal from a Single Image using LAB Color Space", *Cybernatics and Information Technologies,* 13(1), pp. 95-104 (2013).

[2] Selvi, N. M. "Shadow Detection and Removal in Color Images using MATLAB", *International Journal for Trends in Engineering & Technology,* 06(1), pp. 205-208 (2015).

[3] Tiwari, A. Singh, P. K. and Amin, S. "A Survey on shadow detection and removal in images and viedo sequences", *International Conference on Cloud system and Big data Engineering,* pp. 518-523 (2016).

[4] Wang, J. M. Chung, Y. C. Chang, C. L. and Chen, S. W. "Shadow dettection and removal for traffic images", *International Conference on Networking, sensing and control,* 1, pp. 649-654 (2004).

[5] Bansal, N. Akashdeep and Aggarwal, N. "Deep Learning based shadow detection in images", *International Conference on communication, computing and networking,* 46, springer, Singapore (2019).

[6] Mohajerani, S. and Saeedi, P. "CPNet: A Context Preserver Convolutional Neural Network for Detecting Shadows in Single RGB Images", *(MMSP 2018) IEEE 20th International Workshop on Multimedia Signal Processing,* (29-31, Aug. 2018).

[7] Zigh, E. Belbachir, M. F. Kadiri, M. Djebbouri, M. and Kouninef, B. "New Shadow Detection and Removal approach to improve neural stereo corresponence of dense urban VHR remote sensing images", *European Journal of Remote Sensing,* 48(1), pp. 447-463 (2017).

[8] Paul M., D. "Shadow analysis in high-resolution satellite imagery of urban areas", *Photogrammetric Engineering and Remote Sensing,* 71(2), pp. 169-177 (2005).

[9] Tsai, V.U.D. "A comparative study on shadow compensation of color aerial images in invariant color models", *IEEE Transactions on Geoscience and Remote Sensing,* 44(6), pp 1661-1671 (2006).

[10] Krishna, K.S. Kirat P. and Nigam, M.J. "Shadow detection and removal from remote sensing images using NDI and morphological operators", *International Journal of Computer Applications,* 42(10), pp. 37-40 (2012).

[11] Finlayson, G. D. Drew, M. S. and Lu, C. "Entropy Minimization for Shadow Removal", Int. J. Comput. Vision, 85(1), pp. 35-57 (2009).

[12] Miyazaki, D. Matsushita, Y. and Ikeuchi, K. "Interactive Shadow Removal from a Single Image Using Hierarchical Graph Cut", *In: Proceedings of 9th Asian Conference on Computer Vision,* Springer-Verlag, Berlin, Heidelberg, 01, pp. 234-245 (2010).

[13] Zhu, J. Samuel, K. G. G. S. Masood, Z. and Tappen, M. F. "Learning to Recognize Shadows in MonoChromacity based method Natural Images", *In: CVPR, IEEE,* pp. 223-230 (2010).

[14] Prati, A. Mikic, I. Trivedi, M. and Cucchiara, R. "Detecting moving shadows: algorithms and evaluation", *IEEE Transactions on Pattern Analysis and Machine Intelligence,* 25(7), pp. 918–923 (2003).

[15] Mitra, B. Young, R. and Chatwin, C. "On shadow elimination after moving region segmentation based on different threshold selection strategies", *Optics and Lasers in Engineering,* 45(11), pp. 1088–1093 (2007).

[16] Sanin, A. Sanderson, C. and Lovell, B. C. "Shadow Detection: A Survey and comparitive Evaluation of Recent Methods", *Pattern Recognition,* 45(4), pp. 1684-1695 (2012).

[17] Cucchiara, R. Grana, C. Piccardi, M. and Prati, A. "Detecting moving objects, ghosts, and shadows in video streams", *IEEE Transactions on Pattern Analysis and Machine Intelligence,* 25(10), pp. 1337–1342 (2003).

[18] Salvador, E. Cavallaro, A. and Ebrahimi, T. "Cast shadow segmentation using invariant color features", *Computer Vision and Image Understanding,* 95(2), pp. 238–259 (2004).

[19] Cavallaro, A. Salvador, E. and Ebrahimi, T. "Shadow-aware object-based video processing", *IEE Proceedings on Vision, Image and Signal Processing,* 152(4), pp. 398–406 (2005).

[20] Shoaib, M. Dragon, R. and Ostermann, J. "Shadow detection for moving humans using gradient-based background subtraction", *In IEEE International Conference on Acoustics, Speech and Signal Processing,* pp. 773–776 (2009).

[21] Chen, C.-C. and Aggarwal, J. "Human shadow removal with unknown light source", *In International Conference on Pattern Recognition,* pp. 2407–2410 (2010).

[22] Chen, C.-T. Su, C.-Y. and Kao, W.-C. "An enhanced segmentation on vision-based shadow removal for vehicle detection", *In International Conference on Green Circuits and Systems,* pp. 679–682 (2010).

[23] Huang, J.-B. and Chen, C.-S. "Moving cast shadow detection using physics-based features. In IEEE Conference on Computer Vision and Pattern Recognition", pages 2310–2317 (2009).

[24] Martel-Brisson, N. and Zaccarin, A. "Kernel-based learning of cast shadows from a Huang and chen method [23] model of light sources and surfaces for low-level segmentation", *In IEEE Conference on Computer Vision and Pattern Recognition,* pages 1–8 (2008).

[25] Nadimi, S. and Bhanu, B. "Huang and chen method [23] models for moving shadow and object detection in video" *IEEE Transactions on Pattern Analysis and Machine Intelligence,* 26(8), pp. 1079–1087 (2004).

[26] Pei, L. and Wang, R. "Moving cast shadow detection based on PCA", *In International Conference on Natural Computation*, 2, pp. 581–584 (2009).

[27] Shoaib, M. Dragon, R. and Ostermann, J. "Shadow detection for moving humans using gradient-based background subtraction", *In IEEE International Conference on Acoustics, Speech and Signal Processing*, pp. 773–776 (2009).

[28] Sanin, A. Sanderson, C. and Lovell, B. "Improved shadow removal for robust person tracking in surveillance scenarios", *In International Conference on Pattern Recognition,* pp. 141–144, 2010. DOI: 10.1109/ICPR.2010.43.

[29] Mallet, S. "A Wavelet Tour of Signal Processing", Academic Press, New York (1998).

[30] Donoho, D. L. "De-noising by soft thresholding", IEEE Trans. Inform. Theory", 41, pp. 613–627 (1995).

[31] Boyat, A. and Joshi, B. K. "A Review Paper: Noise Models in Digital Image Processing", *Signal & Image Processing: An International Journal (SIPIJ),* 06(02), (2015).

[32] Joshi, A. Boyat, A. and Joshi, B. K. "Impact of Wavelet Transform and Median Filtering on Removal of Salt and Pepper Noise in Digital Images", *IEEE International Conference on Issues and Challenges in Intelligent Computing,* Gaziabad, pp. 838 – 843 (2014).

[33] Yoneyama, A. Yeh, C. and Kuo, C. "Moving cast shadow elimination for robust vehicle extraction based on 2d joint vehicle/shadow models", In IEEE Conference on Advanced Video and Signal Based Surveillance, pp. 229–236 (2003).

[34] Javed, O. and Shah, M. "Tracking and object classification for automated surveillance", *In Proc. European Conf. Computer Vision,* 4, pp. 343–357 (2002).

[35] Joshi, A. and Papanikolopoulos, N. "Learning to detect moving shadows in dynamic environments", *IEEE Transactions on Pattern Analysis and Machine Intelligence,* 30(11), pp. 2055–2063 (2008).

[36] Martel-Brisson, N. and Zaccarin, A. "Learning and removing cast shadows through a multidistribution approach", *IEEE Transactions on Pattern Analysis and Machine Intelligence,* 29(7), pp. 1133–1146 (2007).

[37] Leone, A. and Distante, C. "Shadow detection for moving objects based on texture analysis", Pattern Recognition, 40(4), pp. 1222–1233 (2007).

[38] Fang, L. Z. Qiong, W. Y. and Sheng, Y. Z. "A method to segment moving vehicle cast shadow based on wavelet transform", *Pattern Recognition Letters,* 29(16), pp. 2182–2188 (2008).

[39] Nicolas, H. and Pinel, J.-M. "Joint moving cast shadows segmentation and light source detection in video sequences", *Signal Processing: Image Communication,* 21(1), pp. 22–43 (2006).

[40] Liu, Z. Huang, K. Tan, T. and Wang, L. "Cast shadow removal combining local and global features", *In IEEE Conference on Computer Vision and Pattern Recognition*, pp. 1–8 (2007).

[41] Pei, L. and Wang, R. "Moving cast shadow detection based on PCA", *In International Conference on Natural Computation*, 2, pp. 581–584 (2009).

[42] Hsieh, J.-W. Hu, W.-F. Chang, C.-J. and Chen, Y.-S. "Shadow elimination for effective moving object detection by Gaussian shadow modeling", *Image and Vision Computing,* 21(6), pp. 505–516(2003).

Dr. Ajay Kumar Boyat is Sr. Assistant Professor in Electronics & Communication Engineering at Medi-Caps University, Indore (M.P.), India. He has completed B.E. in Electronics and Communication Engineering from MITS, Gwalior in 2005, M.E. in Electronics and Telecommunication Engineering from SGSITS, Indore in 2008 and Ph.D. in Electronics and Telecommunication Engineering from

Research center Military College of Telecommunication Engineering, Devi Ahiliya University, Indore, INDIA. His research interests are Image processing, Adaptive and Non-Linear Filtering, Signal Processing, Wavelet Neural Network, Mobile adhoc and Wireless Communication networks. He has number of research papers to his credit and has supervised three Post Graduate scholar and currently supervising three Post Graduate scholars. He has 12 years of teaching and industry experience. He has a Research and Project Cordinator in Department of Electronics & Communication Engineering at Medi-Caps University, Indore (MP), India. He is a Global member of Internet Society. He has received certificate of Honour as a Teacher achieve excellence in the subject Material Science (ES220) and Microprocessor and Microcontroller (EC5003), from SRIJAN (Festival of Technical papers and Innovative models), during 2016-2017 and 2017-2018, respectively. He has received Best Paper Award from IEEE PODHIGAI and IEEE SIPCICOM in IEEE International Conference on Computational Intelligence and Computing Research, Dec. 18-20, 2014.